Mon. Not. R. Astron. Soc. **000**, 000–000 (2001)

A comparison of DA white dwarf temperatures and gravities from Lyman and Balmer line studies

M.A. Barstow[1], J.B. Holberg[2], I. Hubeny[3], S.A. Good[1], A.J. Levan[1] and F. Meru[4]
[1] *Department of Physics and Astronomy, University of Leicester, University Road, Leicester LE1 7RH, UK*
[2] *Lunar and Planetary Laboratory, University of Arizona, Tucson, AZ 85721, USA*
[3] *Laboratory for Astronomy and Solar Physics, NASA/GSFC, Greenbelt, Maryland, MD 20711 USA*
[4] *Nottingham High School for Girls, 9 Arboretum Street, Nottingham NG1 4JB, UK*

30 July 2001

ABSTRACT

We present measurements of the effective temperatures and surface gravities for a sample of hot DA white dwarfs, using the Lyman line data available from the *HUT*, *ORFEUS* and *FUSE* far-UV space missions. Comparing the results with those from the standard Balmer line technique, we find that there is a general good overall agreement between the two methods. However, significant differences are found for a number of stars, but not always of a consistent nature in that sometimes the Balmer temperature exceeds that derived from the Lyman lines and in other instances is lower. We conclude that, with the latest model atmosphere calculations, these discrepancies probably do not arise from an inadequate theoretical treatment of the Lyman lines but rather from systematic effects in the observation and data reduction processes, which dominate the statistical errors in these spectra. If these systematic data reduction effects can be adequately controlled, the Lyman line temperature and gravity measurements are consistent with those obtained from the Balmer lines when allowance is made for reasonable observational uncertainties.

Key words: stars:atmospheres – stars:white dwarfs – ultraviolet:stars.

1 INTRODUCTION

Two of the most fundamental measurements required to understand the nature of any star are the determination of its surface gravity and effective temperature. In the case of the white dwarf stars, where nuclear burning has long since ceased, temperature is an indication of their cooling age and, therefore, enables us to map out the evolutionary sequence. Early studies of the white dwarf population relied on photometric measurements (e.g. Koester *et al.* 1979). However, a major break through in the reliability and accuracy of these measurements was achieved with the development of a spectroscopic technique for the H-rich DA white dwarfs, pioneered by Holberg *et al.* (1986), where the *IUE* observed H i Lyman α lines of a number of DA white dwarfs were compared with synthetic model stellar atmospheres. Similar techniques can be applied to the H i Balmer lines (Holberg *et al.* 1985). Indeed, when multiple Balmer lines (usually 3 or 4) are systematically analysed a unique well-defined determination of both the temperature and surface gravity can be obtained. Bergeron *et al.* (1992, BSL) were the first to apply this technique to a large sample of DA white dwarfs. Combining the measurements of $T_{\rm eff}$ and $\log g$ with the evolutionary calculations of Wood (1992), BSL obtained estimates of the mass for each star, confirming the narrowness of the white dwarf mass distribution and yielding an accurate measurement of its peak. Subsequent studies of large samples of white dwarfs from both optical and EUV surveys have firmly established this technique as the primary way of determining the DA white dwarf temperature scale and placing these objects in their evolutionary context (see Vennes *et al.* 1997; Marsh *et al.* 1997; Finley *et al.* 1997a).

The Balmer line technique can only be applied if these features are visible in the stellar spectrum. However, there are several situations where this is not the case or where the measurement is compromised in some way. For example, if a white dwarf resides in a binary system with a much more luminous main sequence or evolved companion, the optical spectrum will be dominated by the latter star. A well-known illustration of this is the DA+K star binary V471 Tauri, which has been studied extensively (e.g. Barstow *et al.* 1997 and references therein) and where the Balmer lines are not detectable in the glare of the K2 dwarf. One major result of the EUV sky surveys has been the discovery of many more similar systems with companion spectral types ranging

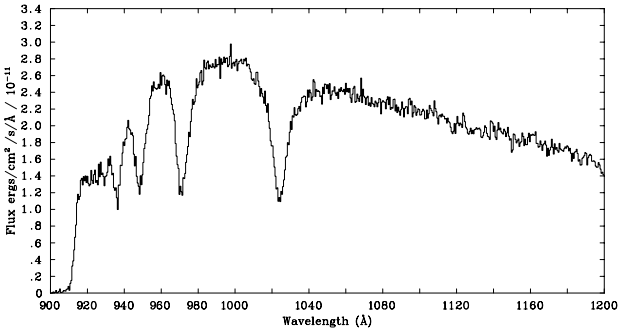

Figure 1. Section of the *HUT* spectrum of G191−B2B, covering the wavelength range from 900Å to 1200Å.

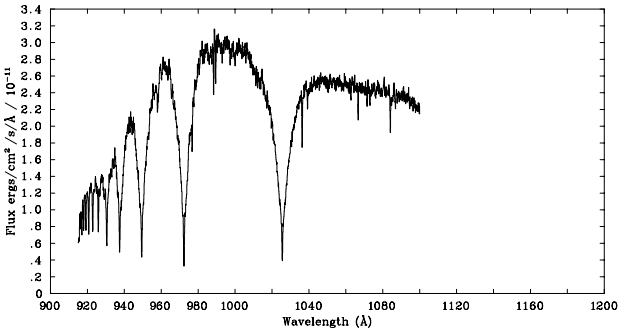

Figure 2. *ORFEUS* spectrum of G191−B2B.

from A to K (e.g. Barstow *et al.* 1994a; Vennes *et al.* 1998; Burleigh *et al.* 1997).

While the signature of the white dwarf cannot be visually separated from its companion in these binaries, the UV flux from the degenerate star dominates that from the late-type star, provided the primary has a spectral type later than $\approx A2$. Consequently, most of the white dwarfs in such systems have been identified from *IUE* spectra. In principle, the white dwarf temperature and gravity can be determined from the Lyman α line profile in each case. However, a single line is unable to give an unambiguous measurement of both $T_{\rm eff}$ and $\log g$ simultaneously. Additional information, such as the stellar distance, can constraint the possible values further, but the distance measurements may not always be sufficiently accurate or may be based on uncertain knowledge of the primary spectral type. The importance of access to the Lyman series in an unresolved binary is illustrated by determination of $T_{\rm eff}$ and $\log g$ for several important white dwarfs including V471 Tauri (Barstow *et al.* 1997) and HZ43 (Dupuis *et al.* 1998), based on spectra obtained by the *ORFEUS* spectrometer (see below). More recently, Burleigh *et al.* (2001) have obtained $T_{\rm eff}$ and $\log g$ for the white dwarf companion to the A star β Crateris, using *FUSE*.

In principle, the full Lyman line series could be used in the same manner as the Balmer lines to determine $T_{\rm eff}$ and $\log g$. While the *IUE* and *HST* bands do not extend to short enough wavelengths to encompass more than Lyman α, the short duration *HUT* and *ORFEUS* missions have provided several observations of white dwarfs down to the Lyman limit with which to examine this idea. The *HUT* telescope was carried into space twice aboard the Space Shuttle, as part of the *Astro 1* and *Astro 2* missions. A total of eight isolated hot DA white dwarfs were observed at a resolution of ≈ 4Å (fwhm). Launched from the Space Shuttle, the *ORFEUS* missions utilised a free-flying far-UV spectrometer operating at a factor 10 higher resolution (≈ 0.3Å) than *HUT*. A total of four DAs were observed during two separate flights.

Several authors have used these far-UV spectra to determine $T_{\rm eff}$ and $\log g$. However, as the total number of stars studied on any one mission has been small, it has been difficult to establish whether or not the results of Lyman line analyses are generally in agreement with Balmer line observations of the isolated DA stars. A test of this nature is crucial if we are to routinely use Lyman line data for this purpose. A preliminary investigation of this issue was carried out by Finley *et al.* (1997b), using the *Astro 2 HUT* data. Their major conclusion was that the Lyman lines were significantly weaker than the standard Stark broadening theory of Vidal *et al.* (1973). Conflicting results have been obtained with the *ORFEUS* data. For example, Barstow *et al.* (1998), utilizing state-of-the-art non-LTE models, found that the Lyman and Balmer $T_{\rm eff}$ determinations were in good agreement for the heavy element rich star G191−B2B but not for the similar object REJ0457−281. Dupuis *et al.* (1998) also achieved good agreement between the results of their Lyman line analysis of the pure H atmosphere white dwarf HZ43 and other published values of $T_{\rm eff}$ from a variety of published sources including *HUT*, *EUVE* besides ground-based Balmer line observations. However, it must be remembered that these measurements reported in the literature were derived using several different model codes, spanning several generations of these programmes. Hence, such comparisons lack the uniformity and self-consistency required to evaluate the efficacy of the Lyman lines as reliable $T_{\rm eff}$ and $\log g$ indicators. The launch of the Far Ultraviolet Spectroscopic Explorer (*FUSE*) on 1999 June 24 has provided long duration access to the Lyman series region of the electromagnetic spectrum for the first time since Copernicus, in the early 1970s. However, Copernicus was not sufficiently sensitive to observe any white dwarfs, except Sirius B. With a spectral resolution superior to both *HUT* and *ORFEUS*, and comparable effective area, *FUSE* promises to produce Lyman series data for many white dwarfs. This paper presents a critical analysis of the use of the H Lyman series absorption lines to determine $T_{\rm eff}$ and $\log g$. We reanalyze the archival *HUT* and *ORFEUS* spectra in conjunction with new, improved non-LTE synthetic spectra, comparing the results with our archive of Balmer line data, using the same models. We also consider the possible systematic observation and data reduction effects that might affect either or both Balmer and Lyman procedures.

Table 1. Far-UV Lyman series spectra used in this study, obtained from *HUT*, *ORFEUS* and *FUSE* missions.

Star	Instrument	Data set name/number
GD50	*HUT*2	A19001, A19002
GD394	*HUT*2	A09201, A09202, A13801, A21101
HZ43	*HUT*	A32901, A32902
	*ORFEUS*2	12, 3270659-3362240
REJ0512	*HUT*2	A12701, N12701
G191−B2B	*HUT*2	N11401
	*ORFEUS*1	4, g191b2b_1-4
GD153	*FUSE*	M1010401
GD71	*HUT*2	N11201
	FUSE	M1010301, M1010302
REJ0457	*ORFEUS*1	4, mct0455_1-4
PG1342+444	*FUSE*	A0340402
REJ0558	*FUSE*	A0340701
REJ1738	*FUSE*	A0340301

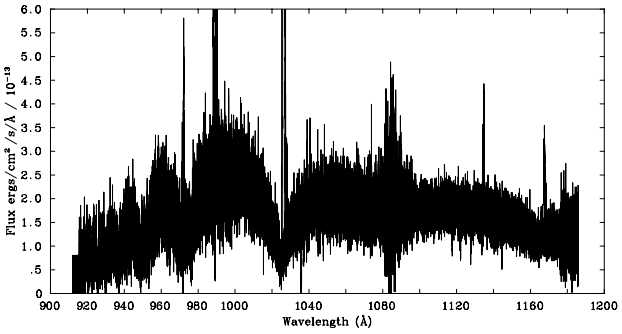

Figure 3. *FUSE* spectrum of PG1342+444, a) combined from the individual grating spectra, before applying our processing pipeline.

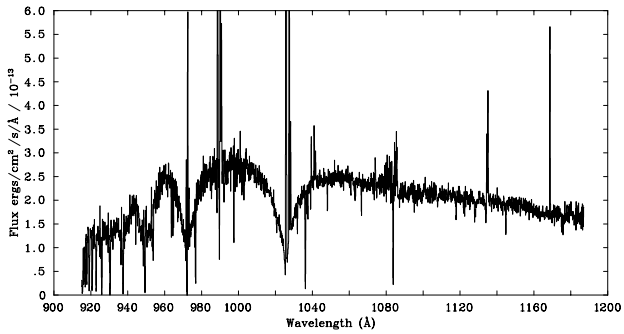

b) After processing, as described in the text and resampled with a 0.1Å bin size to improve the s/n.

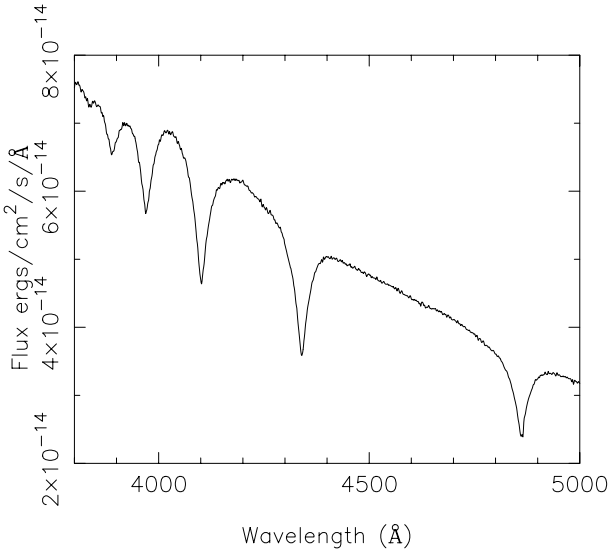

Figure 4. Ground-based optical spectrum of GD71.

2 OBSERVATIONS

2.1 Lyman line spectra

We have obtained far-UV spectra covering the Lyman series from the β line through to the series limit from three telescopes, *HUT*, *ORFEUS* and *FUSE*. Table 1 summarises all the observations, which are discussed briefly below. All the spectra were obtained from the Multi-mission archive (MAST, http://archive.stsci.edu/mast.html) hosted by the Space Telescope Science Institute, or directly from the investigators of the respective instruments.

2.1.1 HUT observations

The *HUT* instrument was flown on two space shuttle missions, *Astro 1* and *Astro 2*, in 1990 December and 1995 March respectively. The payload consisted of a 90cm f/2 telescope with a Rowland circle spectrograph at the prime focus, covering the 820-1840Å wavelength range, in first order. The spectral resolution ($\lambda/\Delta\lambda = 500$) was dependent upon the instrument temperature and pointing stability. The final calibration is described by Kruk *et al.* (1997).The second flight incorporated significant improvements in sensitivity and stability. The spectral resolution was wavelength dependent in this flight, varying from 2-4.5 Å (fwhm). Both temporal and wavelength dependent sensitivity changes were experienced during the mission, which were monitored and characterized by multiple observations of three white dwarfs. Kruk *et al.* (1999) discuss the final *Astro 2 HUT* calibration. An example *HUT* spectrum, of G191-B2B, is shown in figure 1 While eight stars were observed, in REJ1738 strong H_2 absorption prevents sensible analysis of the H Lyman lines (the increased resolution allows the H_2 lines to be removed in the *FUSE* spectrum). In addition, Wolf 1346 is too cool to show a full Lyman line series and is not suitable for this study. Hence, we only made use of observations of six stars.

2.1.2 ORFEUS observations

Higher resolution far-UV spectra were obtained with the *ORFEUS* telescope (Hurwitz & Bowyer 1991) on the free-flying *Astro-SPAS* platform, deployed from the shuttle. *ORFEUS* was flown on two occasions, a 5 day mission in 1993 September and a 14 day mission in 1996 November. On the

first flight, the Berkeley spectrometer located at the focus of the 1-m primary, covered the spectral range 360-1176Å at a resolution of $\lambda/\Delta\lambda = 5000$ (Hurwitz & Bowyer 1995; Hurwitz *et al.* 1998). For the second mission, the far-UV wavelength coverage was 900-1200Å and the spectral resolving power 3300 (Hurwitz *et al.* 1998).

All data obtained during both *ORFEUS* missions are now in the public domain. The raw spectra suffer from contamination by a scattered light component, which is a combination of EUV flux from the second spectral order and direct scatter from the grating (Hurwitz, private communication). When added to the stellar spectrum, the apparent level of the continuum flux will be higher than the true one. In determinations of $T_{\rm eff}$ and $\log g$, the line profiles, whether Balmer or Lyman, are measured from the continuum level. Therefore, the scattered light component must be accounted for in any analysis to avoid obtaining erroneously high temperatures from apparently weaker lines. Immediately shortward of the Lyman limit, the stellar spectrum makes no contribution to the net flux, as a result of absorption by interstellar neutral hydrogen. Therefore, the level of the scattered light component was estimated from the observed flux in the 850–900Å range. The *ORFEUS* spectrum of G191−B2B is shown in figure 2, for comparison with the *HUT* spectrum (figure 1). While four stars were observed, one of these, the white dwarf in V471 Tauri is in a close binary and no Balmer series data can be obtained due to the overwhelming brightness of the K star companion.

2.1.3 FUSE spectra

The *FUSE* mission was placed in low Earth orbit on 1999 June 24. After several months of in-orbit checkout and calibration activities, science observations began during 1999 December. An overview of the *FUSE* mission has been given by Moos *et al.* (2000) and the spectrograph is described in detail by Green *et al.* (1994). Further useful information is included in the *FUSE* Observer's Guide (Oegerle *et al.* 1998) which can be found with other technical documentation on the *FUSE* website (http://fuse.pha.jhu.edu).

Only a few scientific papers have, as yet, been published incorporating *FUSE* data. Hence, it is appropriate to give a brief description of the spectrometer and its current status in the context of the reduction and analysis of the data presented here. The far-UV spectrometer is based on the Rowland circle design and comprises four separate optical paths (or channels). Each channel consists of a mirror, a focal plane assembly (including the spectrograph apertures), a diffraction grating and a section of one of two detectors. To maximise the throughput of the instrument, the channels must be co-aligned so that light from a single target properly illuminates all four channels. Two of the mirrors and two of the gratings are coated with SiC to provide sensitivity at wavelengths below ≈ 1020Å, while the other two mirror/grating pairs are coated with Al and a LiF overcoat. This latter combination yields about twice the reflectivity of SiC at wavelengths above 1050Å, but has little reflectivity below 1020Å. The overall wavelength coverage runs from 905Å to 1187Å.

Spectra from the four channels are recorded on two microchannel plate detectors, with a SiC spectrum and LiF spectrum on each. The individual detectors are divided into two functionally independent segments (A and B), separated by a small gap. Consequently, there are eight detector segment/spectrometer channel combinations to be dealt with in reducing the *FUSE* data. The nominal wavelength ranges of these are listed in table 2.

Table 2. Nominal wavelength ranges (Å) for the *FUSE* detector segments

Channel	Segment A	Segment B
SiC 1	1091.1–1003.9	992.6–905.0
LiF 1	987.1–1082.2	1094.3–1187.7
SiC 2	916.8–1006.4	1016.3–1105.0
LiF 2	1181.7–1085.6	1074.6–978.1

Several problems have been reported during in-orbit operations of the *FUSE* satellite which need to be taken into account in the data reduction process. Maintaining the co-alignment of the individual channels has been difficult, probably due to thermal effects. Sometimes, during an observation, a target may completely miss the aperture of one or more channels, while being well centred in the others. In addition, even if the channels are well-aligned at the beginning of an observation, the target may subsequently drift out of any of the apertures. To minimize this problem, most observations have been conducted using the largest aperture available (LWRS, 30 × 30 arcsec), limiting the spectral resolution for point sources to between 10000 and 20000 (≈ 0.05 to 0.1Å) compared to the 24000-30000 expected for the 1.25 × 20 arcsec HIRS aperture.

Most of the *FUSE* spectra included in this work were obtained in time-tag mode (where the arrival time of each detected photon is recorded and the image subsequently reconstructed from the positional data also included in the data stream) in several separate exposures through the LWRS aperture (table 1). However, two observations (GD71 and GD153) were obtained from the MAST archive as part of the early release of data for calibration purposes. All these data were processed with the CALFUSE pipeline version 1.6.6. Subsequently, a new wavelength calibration has been made available and which is applied to all data processed recently (pipeline version 1.7). We have replaced the original wavelength calibration files with the revised versions according to the procedure described on the *FUSE* data analysis web pages (fuse.pha.jhu.edu/analysis/wavelength_062200.html), before combining the individual spectra.

Initially, for each star, we considered the separate exposures for a single channel/detector segment. Since, the signal-to-noise of these is relatively poor and the wavelength binning (≈ 0.006Å) over samples the true resolution by a factor of 2-3, all the spectra were rebinned to 0.02Å pixels for examination. Fortuitously, several prominent interstellar absorption lines are detected in each spectrum showing that, for a given channel and detector side, the wavelength scales of each exposure are well aligned. Consequently, it is a straightforward process to co-add the individual exposures, to produce a single spectrum. We used the iraf script FUSECOMBINE (see fuse.pha.jhu.edu/analysis/IRAF_scripts.html) to co-add the multiple exposures, which weights the individual spectra by

their exposure time. This whole procedure was repeated for all eight channel/detector side combinations for each star.

Since the complete *FUSE* wavelength range is covered in 3 $\approx$ 100Å bands, a number of the individual detector segments overlap almost completely in wavelength. For example, the SiC 1A, SiC 2B, LiF 2A and LiF 2B all cover the range $\approx 1000-1100$Å, while the SiC 2A/2B ($\approx 900-1000$Å) and LiF 1A/1B ($\approx$ 1100 − 1200Å) match in wavelength. Consequently, to achieve the optimum signal-to-noise for analysis of the data, it is desirable to combine all these individual segment spectra. We have written a small Fortran programme to do this, which is able to take into account the differing wavelength ranges and spectral bin sizes of each. First, all the spectra are re-sampled onto a common wavelength scale and then re-binned into 0.02Å steps to reduce the level of over sampling and avoid any fringing effects that might arise from the first part of the procedure. The re-sampled/re-binned spectra are then co-added, weighting individual data points by the statistical variance, averaged over a 10Å interval, to take into account the differences in effective area of each segment and any differences in exposure time that may have arisen from rejection of bad data segments. We find, through visual inspection of the observed spectra, that the statistical noise tends to increase towards the edges of the wavelength range. In cases where the signal-to-noise is particularly poor in these regions, we have trimmed the spectra to remove these data points prior to co-addition.

As an example, the *FUSE* spectrum of PG1342+444 is shown in figure 3a, combined from the individual grating spectra but without any of the processing described above. The strong high flux spikes are geocoronal emission lines, while poor s/n regions of the spectrum (usually covered by only one grating) are revealed by increased scatter in the data points (e.g. near 1080Å). A few of the stronger heavy element and interstellar absorption lines are also visible. The broad dip in the 1160-1180Å region of the spectrum is an artefact known as the "worm", which is a local 10-20% reduction in the effective area and produces a corresponding loss of flux. Figure 3b shows the same spectrum processed according to our prescription and resampled with a bin size of 0.1Å to improve the s/n for our analysis.

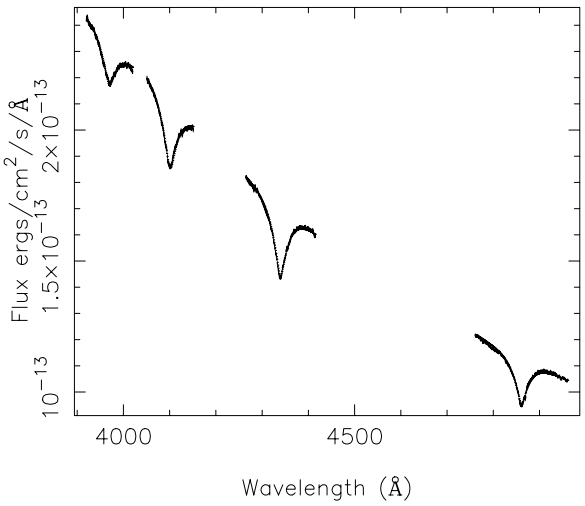

Figure 5. Fit to the ground-based optical Hβ to Hϵ lines of G191−B2B ($T_{\rm eff} = 51510 \pm 880$K, $\log g = 7.53 \pm 0.09$).

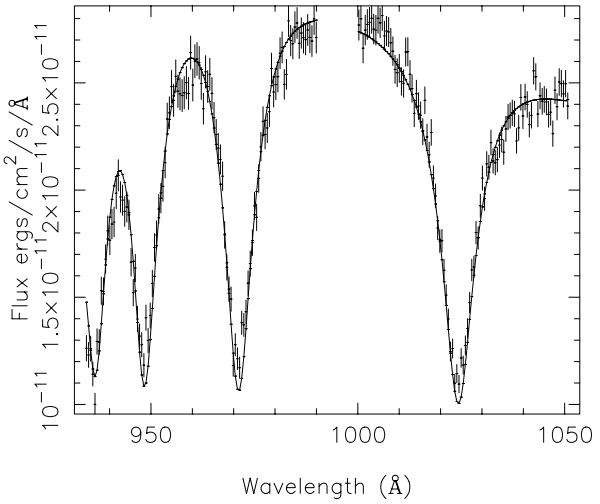

b) Fit to the *HUT* Lβ to Lϵ lines of G191−B2B ($T_{\rm eff} = 52930 \pm 360$K, $\log g = 7.16 \pm 0.20$). Although the line cores are not included in the analysis, they are shown here for illustrative purposes.

2.2 Balmer line spectra

.

The majority of the optical data we use here was obtained as part of a spectroscopic follow-up programme following the *ROSAT* X-ray and EUV sky survey. Observations were undertaken in both Northern and Southern hemispheres. Southern hemisphere data were obtained with the 1.9-m Radcliffe reflector of the South African Astronomical Observatory (SAAO), while stars in the Northern Hemisphere were observed with the Steward Observatory 2.3-m telescope on Kitt Peak. Full details of these observations have already been published by Marsh *et al.* (1997). The main difference between the Southern and Northern Hemisphere data is their spectral resolution, ≈ 3Å (FWHM) and ≈ 8Å (FWHM) respectively. Some of our original Northern Hemisphere spectra did not cover the complete Balmer line series, excluding Hβ, due to the limited size of the CCD chip available at the time. Hence, in those cases, we have replaced the archival data with more recent observations (GD394 and GD71) made using the same instrument but with a larger chip (see e.g. figure 4). For some stars (GD50, HZ43, G191−B2B, and GD153), while archival ("old") data are of good quality and cover all the Balmer line series the "new" observations have longer exposures and, consequently, better s/n. We analyse all these data, as they provide a useful test of consistency between repeated observations of the same star, using basically the same instrument configuration but on different nights.

3 MODEL ATMOSPHERE CALCULATIONS

One potential flaw in comparing the results from published Lyman and Balmer line analyses is that different authors may have utilized different stellar atmosphere codes, even

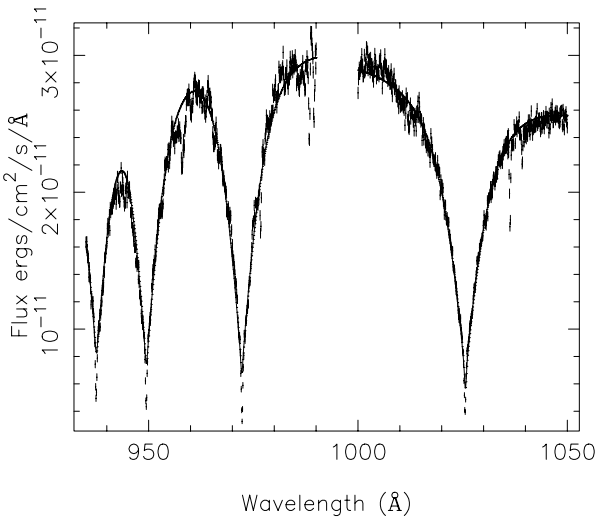

c)

Fit to the *ORFEUS* Lβ to Lϵ lines of G191−B2B ($T_{\rm eff}$ = 53180 ± 520K, $\log g = 7.43 \pm 0.04$). Although the line cores are not included in the analysis, they are shown here for illustrative purposes.

spanning successive generations of these codes. To ensure that our work is at least internally consistent we re-examine all the Balmer line data with the latest version of the stellar atmosphere programme tlusty and its associated spectral synthesis package synspec .

We have calculated completely new grids of model stellar atmospheres using the non-LTE code tlusty (Hubeny & Lanz 1995). These are based on work reported by Lanz *et al.* (1996) and Barstow *et al.* (1998, 1999). Two separate sets of calculations were performed: pure H models, for those stars without significant abundances of heavy elements, and models with a homogeneous mixture of heavier elements, including C, N, O, Si, Fe and Ni, for the others. The upper limit to the temperature of the pure H models was 70000K, to span the range within which DAs with pure H atmospheres are found, while the heavy element calculations were extended to 120000K, to deal with hotter DA stars, although we note that in this particular study the hottest star we consider is REJ1738, with $T_{\rm eff} \approx$ 70000K. To take account of the higher element ionization stages that are likely to be encountered in the latter objects, we have added new ions of OVI, FeVII/VIII and NiVII/VIII to the model atoms as well as extending the data for important ions such as CIV to include more energy levels. As before, all the calculations were performed in non-LTE with full line-blanketing, including Stark broadening of all the CNO lines.

The stars included in this study are divided into two distinct groups. Those with pure H envelopes, for which we used the pure H model calculations, and those with significant quantities of heavy elements. For the latter group, we fixed the abundances of the heavy elements at the values determined from our earlier homogeneous analysis of G191−B2B (He/H=1.0×10^{-5}, C/H=4.0×10^{-7}, N/H=1.6×10^{-7}, O/H=9.6×10^{-7}, Si/H=3.0×10^{-7}, Fe/H=1.0×10^{-5}, Ni/H=5.0×10^{-7}), but taking into account that the CIV lines near 1550Å have subsequently been resolved into multiple components by STIS (Bruhweiler *et al.* 2000; Bannister *et al.* 2001). While not all stars have exactly the same heavy element abundances, our recent work has shown that the differences are not very large (see Barstow *et al.* 2001) and, at this level, will not have a significant effect on the Balmer/Lyman line measurements (see e.g Barstow *et al.* 1998).

In the spectrum synthesis code synspec (Hubeny *et al.* (1994), we have replaced the hydrogen Stark line broadening tables of Schöning & Butler (private communication) by the more extended tables of Lemke (1997). The latter allow a more accurate interpolation of the electron density for high density environments, such as the atmospheres of white dwarfs. The spectra produced by the tlusty /synspec codes were recently extensively tested against the results of Koester's codes (Hubeny & Koester in preparation). The differences in the predicted spectra for $T_{\rm eff}$ =60000K and $\log g = 8$ were found to be below 0.5% in the whole UV and optical range. Furthermore, we have found that the inaccuracy in the interpolations of the Schöning and Butler tables, together with some fine details of our treatment of the level dissolution, were the primary reason for the disagreement between the spectroscopically deduced $T_{\rm eff}$ using tlusty and Koester models obtained by Barstow *et al.* (1998). These changes largely resolve the differences between codes noted by Bohlin (2000).

4 DETERMINATION OF TEMPERATURE AND GRAVITY

The technique for determining $T_{\rm eff}$ and $\log g$, by comparing the line profiles with the predictions of synthetic spectra is well established (see Holberg *et al.* 1986; Bergeron *et al.* 1992 and many subsequent authors). We have described our own Balmer line analysis technique in several earlier papers (e.g. Barstow et al. 1994b), but as the results presented in this paper rely heavily on it we repeat the details here. The same technique can also be applied to analysis of the Lyman lines, as has already been demonstrated (e.g. Barstow *et al.* 1997; Barstow *et al.* 1998). However, we have modified our earlier approach, as outlined below.

Both sets of $T_{\rm eff}$ and $\log g$ measurements were performed using the program xspec (Shafer *et al.* 1991), which adopts a χ^2 minimization technique to determine the model spectrum which gives the best agreement with the data. For the Balmer lines, the four strongest ($\beta, \gamma, \delta, \epsilon$) are simultaneously included in the fit and an independent normalisation constant applied to each, ensuring that the result was independent of the local slope of the continuum and reducing the effect of any systematic errors in the flux calibration of the spectrum. Individual lines maintain their local continuum slope but are decoupled from the overall energy distribution of the entire Balmer line region.

In the case of the Lyman lines, the analysis needs to be handled in a slightly different way. In general, at given values of $T_{\rm eff}$ and $\log g$, the Lyman lines are stronger, and, apart from the α and β lines, overlap substantially. To deal with the Lyman data for each instrument, we separated out the β (1000- 1050Å) line and incorporated the remaining lines (γ through ϵ inclusive) into a single file. To take account of any low frequency systematic effects in the flux calibration we applied individual normalization constants to each of the two sections of data.

Since the Lyman data are, by definition, obtained from

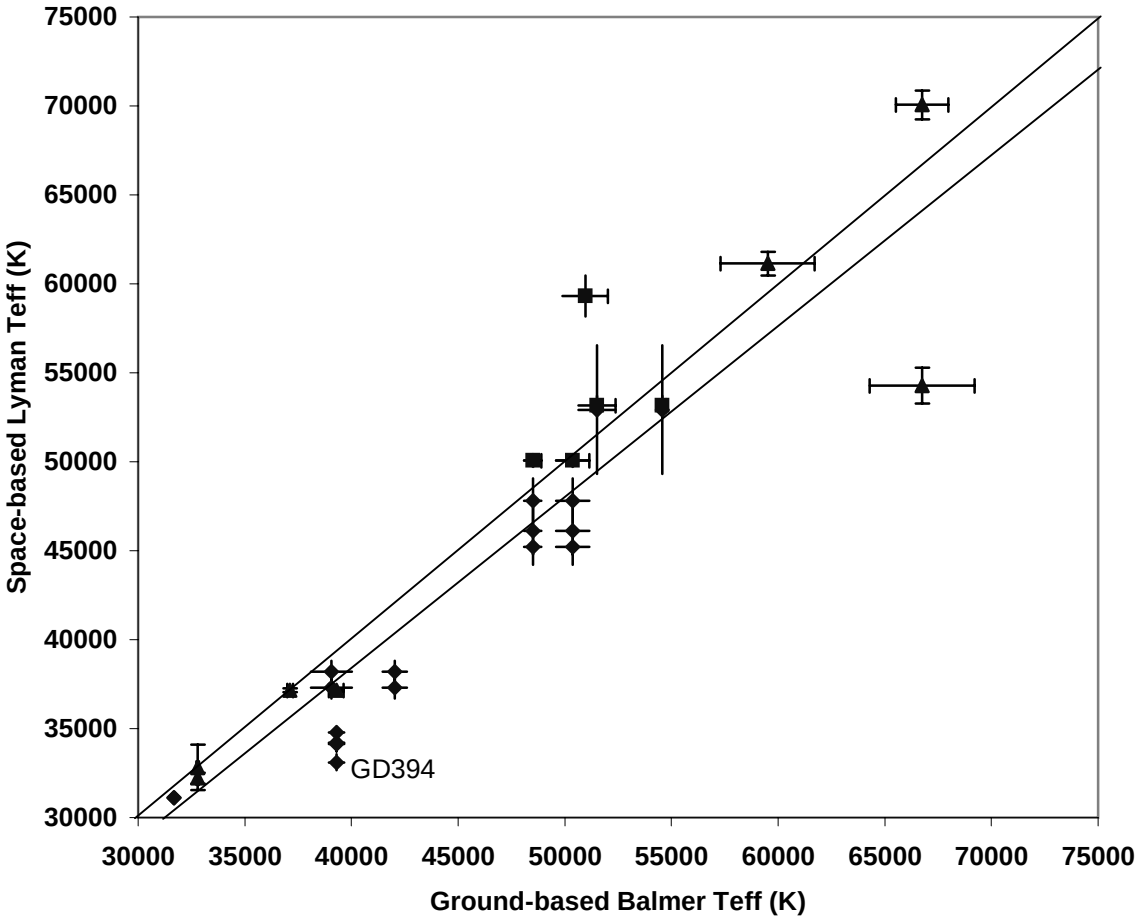

Figure 6. Scatter plot of the values of $T_{\rm eff}$ measured using the Balmer and Lyman series lines. Diamonds are *HUT* data, the squares are the *ORFEUS* data and the triangles the *FUSE* data. The error bars displayed correspond just to the statistical 1σ uncertainties. The upper solid line corresponds to equal Balmer and Lyman temperatures, while the lower line is the least squares straight line fit to the data, corresponding to y=0.964x.

space-based platforms, there are no systematic errors arising from an atmospheric extinction correction. Furthermore, the flux calibration is usually obtained from a detailed off-line calibration of the instrument, applied as part of a standard pipeline, rather than direct comparison of the observed spectrum with that of a selected standard star. However, the instrument calibration still refers to observations of well-studied stars, such as white dwarfs, some systematic uncertainties will still apply, but will be different to those arising from the ground-based techniques Although, in general, no extinction correction needs to be applied to the Lyman series data, there are two important effects that need to be accounted for in any analysis. First, the cores of the Lyman absorption lines can be contaminated by geocoronal emission components. Second, interstellar absorption can artificially deepen the core of the stellar Lyman absorption lines. These two effects compete with each other and may occasionally conspire to cancel each other out, but usually they must be removed from the data in an appropriate way.

The observed strengths of individual geocoronal lines depend on a number of factors, including the strength of the Solar line being scattered, the density of scattering atoms along the line of site (here H i atoms) and the optical depth of the scattering environment. In general however, the strongest line is always Lyman α followed by Lyman β. In most of the data considered here, the Lyman α line is not observed and is only available in the *HUT* data. Hence, it is not used for consistency of analysis and the Lyman β line is by far the strongest component we need to consider (e.g. Figure 3). From a signal-to-noise point of view the relative strength of the emission when compared to the stellar continuum is also affected by the viewing geometry, the instrument design and the brightness of the target star. The geocoronal radiation has a natural spectral width caused by Doppler effects, which is then further broadened in the instrumental aperture by the diffuse nature of the source and the spectral resolution of the instrument. As a result of possible differences in the relative velocity of the stellar and geocoronal sources, the emission lines are not necessarily aligned with the stellar absorption cores.

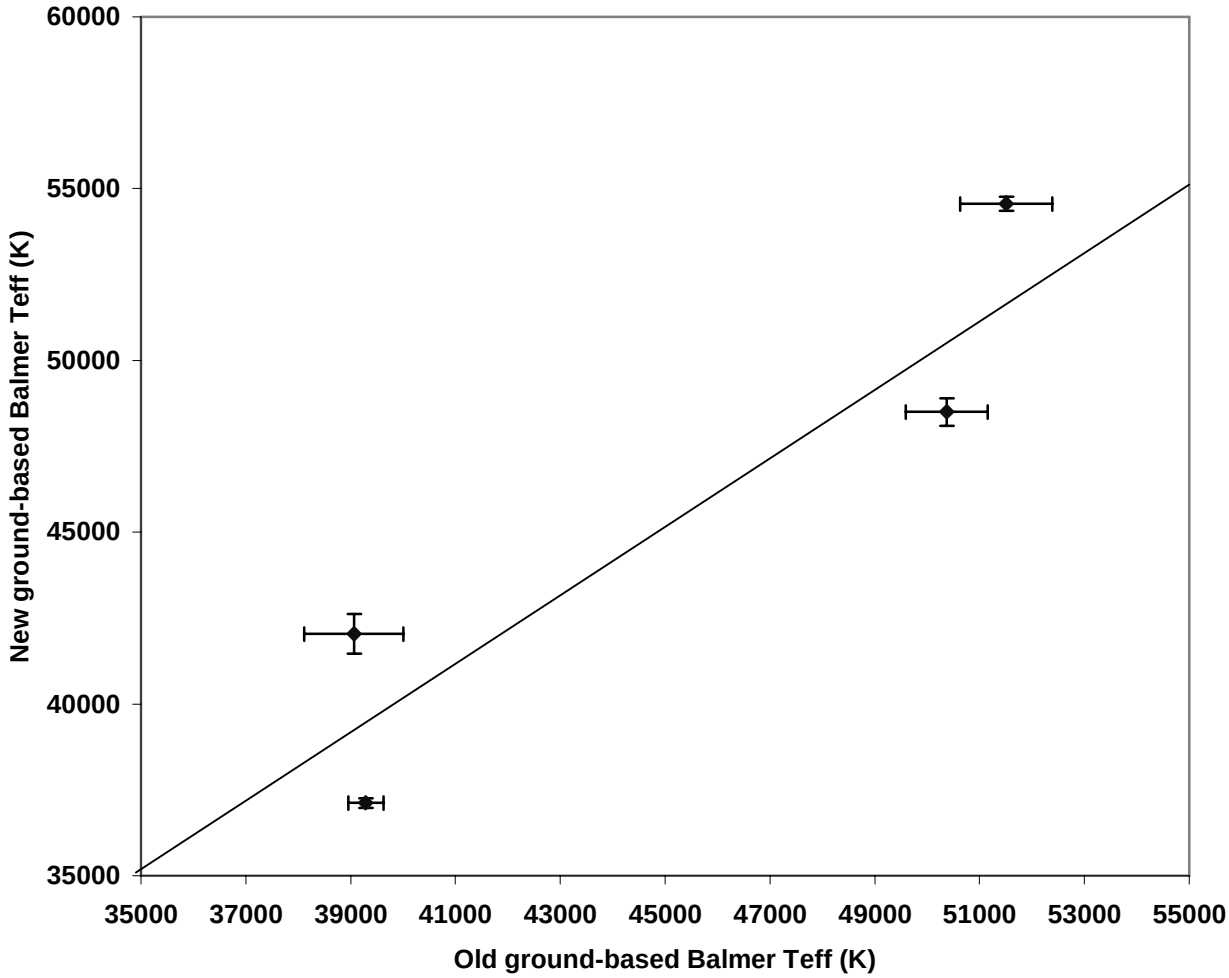

Figure 7. Scatter plot of the values of $T_{\rm eff}$ measured using the "old" (x-axis) and "new" (y-axis) Balmer series lines. The error bars displayed correspond to statistical 1σ uncertainties alone. The light solid line corresponds to equal Balmer temperatures.

To make sensible estimates of the uncertainty in the fitted parameters, the value of the reduced χ^2 should be less than ≈ 2. This is the case for the fits to all the spectra included in this analysis, which are, therefore, formally good fits. Errors on $T_{\rm eff}$ and $\log g$ can then determined by allowing the model parameters to vary until the $\delta\chi^2$ reached the value corresponding to the 1σ level for 2 degrees of freedom (2.3). It should be noted that these estimates only include statistical uncertainties and do not take into account any possible systematic effects related to the data acquisition and reduction processes.

Figure 5 shows examples of the fits to the Balmer (5a) and Lyman (5b, 5c) lines of G191−B2B respectively. G191−B2B is one of only two stars (the other is HZ43), where spectra exist for ground-based, *HUT* and *ORFEUS*, providing a useful cross-check between all these instruments. This is particularly important as, prior to the launch of *FUSE*, the majority of the Lyman line DA data had been obtained by *HUT*.

Table 3 summarises the effective temperatures and gravities obtained from the spectral fits for all data sets for each star, including the 1 σ statistical uncertainties on these values. Where more than one ground-based balmer line measurement is reported, the upper value is obtained with the "old" archival data and the lower is from the "new", higher s/n observation. For GD394 and GD71, the reported measurements are only from the "new" spectra as the archival obervations only span 2-3 lines of the Balmer series and are not used here.

The $T_{\rm eff}$ and $\log g$ measurements obtained from the various observations are a somewhat heterogeneous group. While we have a complete set of ground-based optical spectra for all the stars, and in some cases multiple ground-based observations of an individual star, the far-UV observations are incomplete, with different instruments covering a different group. At this stage, for no star is there a complete set of observations with data from all space-based instruments. In a number of cases, there are multiple observations of a star made with a single telescope. Rather than combine these spectra into a single average, where the signal-to-noise

Table 3. Best-fit effective temperature and surface gravity for each observation of each DA white dwarf in the sample. Multiple values given each column refer to independent observations using the same instrument.

STAR	GROUND BASED		*HUT*		*ORFEUS*(o)/*FUSE*(f)	
	$T_{\rm eff}$ (K) (err)	$\log g$ (err)	$T_{\rm eff}$ (K) (err)	$\log g$ (err)	$T_{\rm eff}$ (K) (err)	$\log g$ (err)
GD50	39060(950)	9.30(0.12)	37300(600)	8.81(0.19)		
	42040(570)	9.15(0.05)	38200(600)	8.82(0.18)		
GD394	39290(360)	7.89(0.05)	34790(300)	7.96(0.10)		
			33100(450)	7.63(0.15)		
			34200(500)	8.01(0.10)		
			34150(400)	8.00(0.10)		
HZ43	50370(780)	7.85(0.07)	46100(1300)	7.65(0.09)	(o)50080(290)	8.14(0.05)
	48500(400)	8.05(0.02)	47800(1250)	7.84(0.12)		
			45200(1000)	7.68(0.13)		
RE0512	31670(140)	7.20(0.04)	31100(250)	7.21(0.10)		
			31100(350)	7.19(0.14)		
G191B2B	51510(880)	7.53(0.09)	52930(3600)	7.16(0.20)	(o)53180(520)	7.43(0.04)
	54560(200)	7.60(0.02)				
GD153	39290(340)	7.77(0.05)			(f)37150(100)	8.1(0.03)
	37120(140)	8.02(0.02)				
GD71	32780(65)	7.83(0.02)	31970(150)	7.72(0.07)	(f)32820(1280)	8.85(0.28)
					(f)32220(310)	8.49(0.07)
REJ0457	50960(1070)	7.93(0.08)			(o)59300(1150)	7.57(0.08)
PG1342	66750(2450)	7.93(0.11)			(f)54286(1000)	7.82(0.07)
REJ0558	59510(2210)	7.70(0.14)			(f)61140(660)	7.61(0.05)
REJ1738	66760(1230)	7.77(0.10)			(f)70060(800)	8.00(0.01)

is adequate, we have chosen to analyse these individually to see if any systematic differences may occur between separate observations of the same star with the same instrument. We discuss the comparison of individual groups of data below.

5 DISCUSSION

5.1 Effective temperatures

In figure 6, we show a scatter plot of the values of $T_{\rm eff}$ measured by Balmer line (x-axis) and Lyman line (y-axis) techniques. All combinations of ground and far-UV observations are shown, to illustrate the full range of possible systematic differences. Also shown is the straight line corresponding to equal Balmer and Lyman temperature together with the best fit straight line corresponding to y=0.964x. In general, there is good agreement between the two measurement techniques, but there also exist some clear anomalies. For example, the Lyman line values of $T_{\rm eff}$ for GD394 are consistent with each other, but systematically lower than the Balmer line value ($T_{\rm eff}$ balmer = 39290) by $\approx$ 5000K. Similarly, the value of $T_{\rm eff}$ measured from the Balmer lines of PG1342+444 is 12000K higher than the corresponding Lyman line measurement. However, such differences are not all in the same direction. The Lyman line temperature of REJ0457 is some 8000K higher than the Balmer temperature. In general, the Lyman $T_{\rm eff}$ measurements are about 4% below the Balmer line values. At 50000K, this corresponds to a difference of 2000K, which is of a similar magnitude to many observational errors.

The information included in figure 6 does not discriminate between the source of optical observations used for comparions with the far-UV measurements. Although the number of repeated optical observations is small, it is still relevant to look for systematic differences to assess the magnitude of systematic uncertainties in the determination of $T_{\rm eff}$. Figure 7 compares the Balmer line temperatures measured using "old" spectra from our archive (x-axis) with those of improved s/n from the more recent ("new") observations. It is clear that, compared to the size of the formal errors, the two sets of data, give different results. Observations for the same stars analysed with the same models disagree for all four stars. The differences range from 5-10%, but are not all in the same direction. In fact, the best fit straight

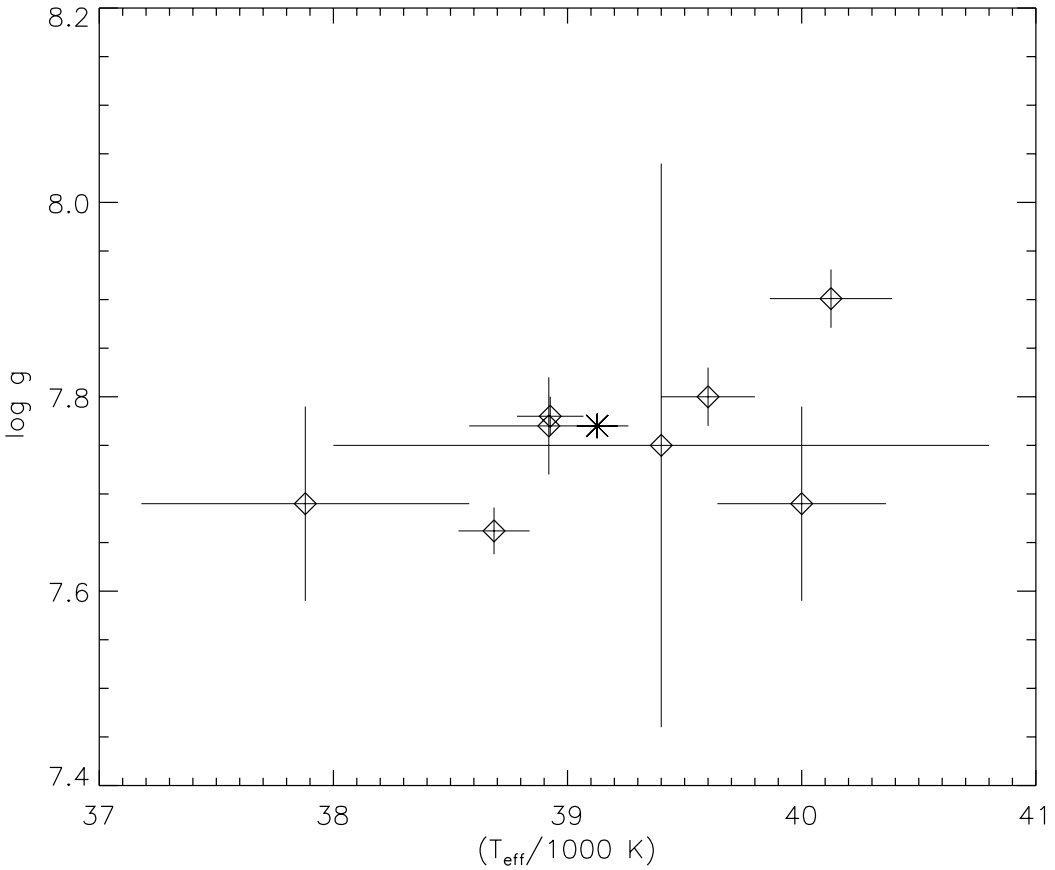

Figure 8. Published independent ground-based Balmer line measurements of $T_{\rm eff}$ and $\log g$ for the white dwarf GD153.

line through the data points is y=1.01x, only 1% different from the ideal y=x. This result would suggest that the ground-based temperature measurements can have systematic errors at the 5–10% level, which dominate the statistical errors in spectra of the signal-to-noise used here. Since $T_{\rm eff}$ and $\log g$ are correlated, similar systematic effects exist for the $\log g$ estimates. This is not a new result and Bergeron *et al.* (1992) use multiple observations of the same star to quantify the systematic errors. The problem is illustrated in figure 8, which shows a summary of spectroscopic observations of GD153. This suggests that, for ground-based $T_{\rm eff}$ and $\log g$ measurements, the statistical uncertainties underestimate the true error by a factor of 2 to 3. Nevertheless, the statistical errors do provide a measure of the spectral s/n, the goodness of fit and the sensitivity of the results to the line strength and should be reported. However, it is not appropriate to take them too literally, particularly when propagating them through calculations such as mass and radius determinations.

Figure 6 shows values of $T_{\rm eff}$ derived from the various Lyman line analyses and each far-UV telescope is denoted by a distinctive symbol (diamonds - *HUT*, squares - *ORFEUS*, triangles - *FUSE*). It is possible to identify particular trends associated with each instrument. Most of the *FUSE* $T_{\rm eff}$ values are in reasonable agreement with the Balmer line measurements. The only dramatic departure is PG1342+444 which, as noted earlier, has a 12000K lower Lyman line temperature. There are too few *ORFEUS* data points, over too narrow a temperature range, to say much about the trends in this instrument. Both HZ43 and G191−B2B are in agreement with the Balmer measurements while the Lyman temperature of REJ0457−281 is 8000K too high. However, we have noted in our earlier work (Barstow *et al.* 1998), that the separate Balmer and Lyman line fits for this star are not, from the point of view of the statistical errors and the goodness of fit (as determined by the F-test described in Barstow *et al.* 1998), significantly different from the average fit to both data sets simultaneously. If we a try a combined fit for PG1342, we do not get the same result: the Lyman, Balmer and combined fits are all significantly different using the same statistical criteria. As discussed earlier in this section, the statistical errors are not a very good indication of the true uncertainty when systematic effects are considered. If we adopt a factor 3 scaling of the statistical errors as representative of the overall analysis process, the level of disagreement between Lyman and Balmer analyses is within 2σ.

Considering the whole sample of observations, the *HUT* data seem to yield Lyman line temperatures that are systematically lower than the Balmer line values. This is most marked in GD394, but is also seen in HZ43 and GD50. Dupuis *et al.* (2000) have already noted this in their detailed study of GD394. Although the discrepancies observed in the other two stars are smaller, it may not be possible to rule out a unique systematic problem with the GD394 data. Hence, the observed temperature effect might not be real.

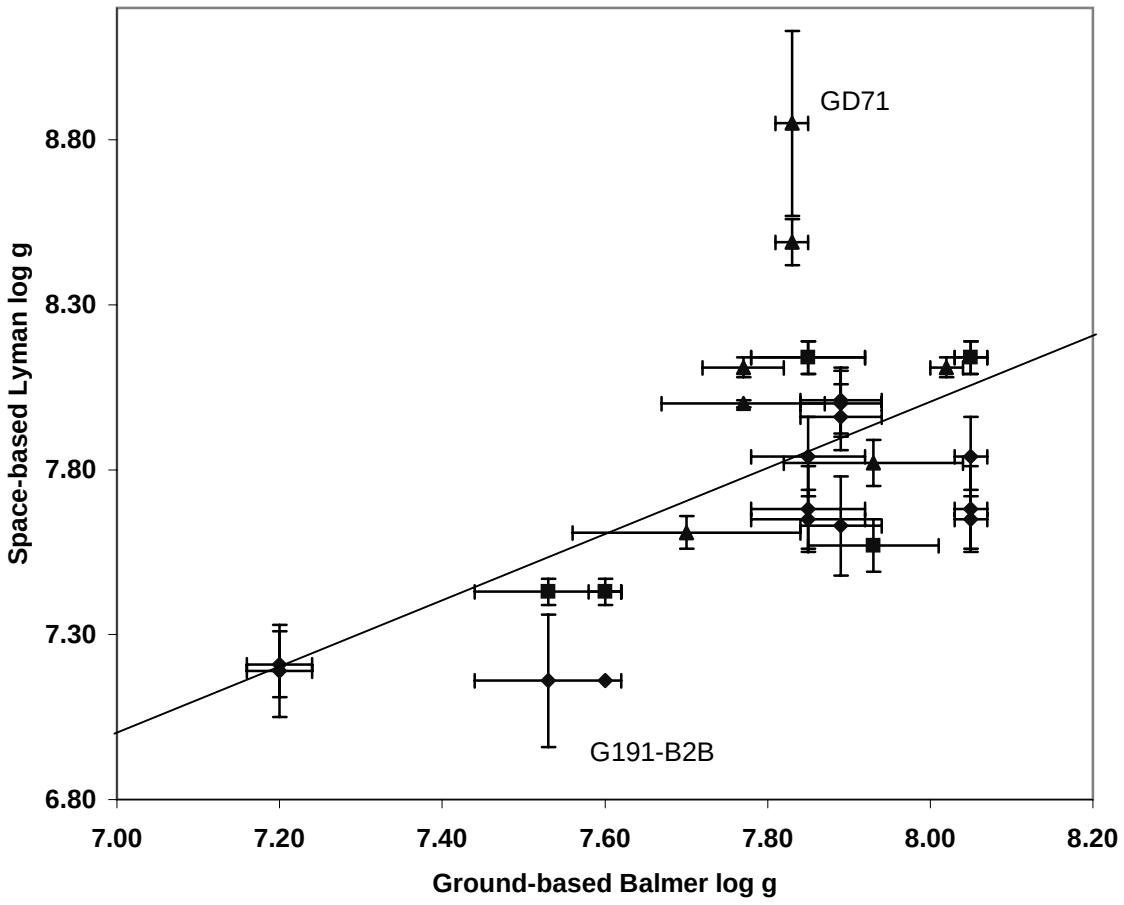

Figure 9. Scatter plot of the values of $\log g$ measured using the ground-based Balmer (x-axis) and far- UV Lyman (y-axis) series lines. The diamonds are *HUT* data, the squares are the *ORFEUS* data and the diamonds the *FUSE* data. The error bars displayed correspond to statistical 1σ uncertainties. The light solid line corresponds to equal Balmer and Lyman line gravities.

The lower resolution of the *HUT* data, when compared to the other instruments pose a particular problem, as outlined earlier, in terms of taking account of geocoronal contamination and interstellar absorption. In addition, removing the entire line cores to eliminate these effects does appear to have a systematic influence on the outcome of the Lyman line analysis.

5.2 Surface gravity measurements

Most of the emphasis of this analysis and discussion has been on the comparison of temperature measurements. However, in determining the evolutionary status and important parameters such as mass and radius, the measurement of surface gravity is of equal importance. Figure 9 shows the measured surface gravities corresponding to the temperature data in figure 6. The fractional statistical errors on $\log g$ are larger than for the temperatures and most error bars overlap the line of equally Balmer and Lyman line gravity. However, there are some marked departures from this. The surface gravity of GD71 obtained from the Lyman line analysis is approximately 1.0dex greater than the Balmer line result, which does not seem reasonable for such a well-studied star. On the other hand the surface gravity measured for G191−B2B is much lower (by 0.37dex) than the Balmer line result. Like the differences in $T_{\rm eff}$ values, these large differences in $\log g$ probably arise from systematic effects in the data. However, there are no apparent trends for any particular instrument and, as in the temperature measurements, no overall systematic departures from the line of equal $\log g$.

5.3 Systematic effects in the analyis of $T_{\rm eff}$ and $\log g$

One of the main propositions of this paper is that measurements of $T_{\rm eff}$ and $\log g$ using either Balmer or Lyman series lines are prone to systematic errors that are not usually well quantified. For the Lyman lines, there is the added complication of geocoronal emission and interstellar absorption modifying the line cores, besides any instrumental effects such as scattered light/background contamination. Consequently, we have simulated some of these effects for selected

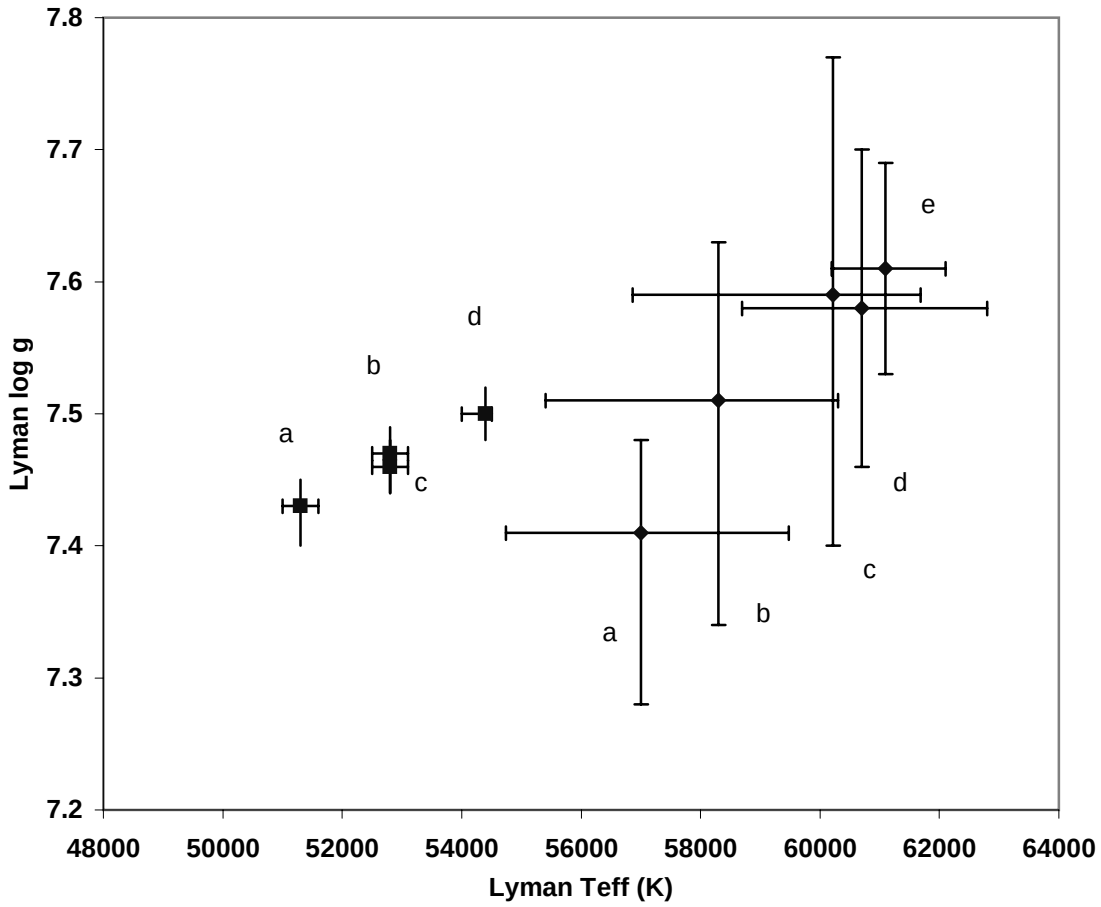

Figure 10. Scatter plot of the values of $T_{\rm eff}$ and $\log g$ measured for the simulated *HUT* (diamonds) and *ORFEUS* (squares) data sets. Each data point is labelled with a letter as indicated in table 4.

HUT and *ORFEUS* data sets to examine the possible contribution to the measurement uncertainties. Fluxes were scaled to analyse the effect of errors in effective area calibrations and constant fluxes were added/subtracted to study the sensitivity to accurate background subtraction/scattered light corrections. For the *HUT* simulation, we also carried out an analysis including the unresolved line cores. In each case, measurements were carried out using the spectral analysis techniques described in section for the real data. Table 4 summarises the results, which are also shown in figure 10.

It is clear that there are significant differences between the measurements of $T_{\rm eff}$ and $\log g$ for each of the simulated datasets. The systematic effects that have been introduced are typically $\approx 5\%$ of the mean flux. These translate into observational errors $\approx 2-5\%$ for $T_{\rm eff}$ and $\approx 0.5-1.0\%$ for $\log g$. While the precision of the *HUT* measurements is similar to the level of the systematic errors, the systematic effects clearly dominate the statistical uncertainties in the *ORFEUS* analyses. It is interesting to note that the total spread of temperature measurements ($\approx$ 10000K) for the simulated data set is as large as some of the perceived discrepancies in the real observations.

6 CONCLUSION

We have measured the effective temperatures and surface gravities for a sample of hot DA white dwarfs using the Lyman line data available from the *HUT*, *ORFEUS* and *FUSE* far-UV space missions, comparing the results with those from the standard Balmer line technique. In general, there is good overall agreement between the two methods. At the level of the pure statistical errors, differences are found between Lyman and Balmer measurements for a number of stars. However, across the sample, the discrepancies are not always in the same direction. This is not what would be expected if the problems arose from limitations of the stellar atmosphere calculations and, in particular, the treatment of Lyman and Balmer line broadening. Hence, while the description of opacity in the region of the Lyman lines is still uncertain, because of uncertainties associated with the occupation probability formalism, the description of the line broadening of the isolated, lower, Lyman lines seems to be in good shape. It is not necessary to make semi-arbitrary adjustments to the input physics, as carried out by Finley *et al.* (1997b) in their analysis of the *HUT* data, to force agreement between the Balmer and Lyman line results. Even so,

Table 4. Values of $T_{\rm eff}$ and $\log g$ measured for the simulated *HUT* and *ORFEUS* data sets. Letter labels correspond to the data points in figure 10.

	HUT simulation	
$T_{\rm eff}$ (K) (err)	$\log g$ (err)	index/comment
57000(2400)	7.41(0.20)	a) basic data
58300(2500)	7.51(0.15)	b) data − constant 5% of mean flux
60220(2300)	7.59(0.14)	c) data scaled by factor 1.05
60700(2050)	7.58(0.12)	d) data + constant 5% of mean flux
61100(950)	7.61(0.08)	e) basic data, but line cores included
	ORFEUS simulation	
$T_{\rm eff}$ (K) (err)	$\log g$ (err)	index/comment
51300(300)	7.43(0.03)	a) data − constant 5% of mean flux
52800(300)	7.47(0.03)	b) basic data
52800(300)	7.46(0.02)	c) data scaled by factor 1.05
54400(250)	7.50(0.02)	d) data + constant 5% of mean flux

there may well be residual second order effects worthy of examination. The best fit line in figure 6 (excluding problematic results noted earlier) hints at a few percent systematic difference between Balmer and Lyman values of $T_{\rm eff}$. However, this is at a similar level to the possible systematic data reduction problems discussed above, which must be eliminated before we can consider this further.

It is well known that optical Balmer line measurements can be sensitive to systematic effects in the data reduction process, in particular the extinction correction that must be applied to take account of atmospheric absorption as well as the absolute flux calibration. Although the former problem is not present in the far-UV spectra it is apparent that this method of temperature and gravity measurement is sensitive to a number of systematic effects that can compromise these results. For example, with the lower spectral resolution *HUT* data, the geocoronal and interstellar contamination of the line cores cannot be dealt with very easily, leading to a systematic shift in measured values of $T_{\rm eff}$. In a simulation, inclusion of the line core regions in the analysis yielded erroneously high values of $T_{\rm eff}$ and $\log g$. In other cases, the accuracy of subtraction of instrument background or scattered light may be important. Simulations of over- or under-subtracted background components at the level of 5% of the mean flux give shifts of similar magnitude in the measured value of $T_{\rm eff}$. With high signal-to-noise data available from a variety of instrumentation, it is clear that our analyses are no longer limited by the statistical errors but by the systematic ones arising in the process of data acquisition and reduction. Consequently, we conclude that, if these effects can be adequately controlled, the Lyman line technique gives measurement that are consistent with those obtained from the Balmer lines, when allowance is made for realistic observational uncertainties.

Acknowledgements

The work reported in the papers was based on observations made with the *HUT*, *ORFEUS* and *FUSE* observatories. We would like to thank Jeff Kruk and Mark Hurwitz for supplying the *HUT* and *ORFEUS* spectra respectively. MAB and SAG were supported by PPARC, UK. JBH wishes to acknowledge support for this work from NASA grants NAG5-9181 and NAG5-8995. FM was supported by a Nuffield Foundation Student Bursary. We would like to thank the referee, Pierre Bergeron, for his very careful critique of this paper and his valuable suggestions for its improvement.

REFERENCES

Bannister N.P., *et al.*, 2001, 12th European Workshop on White Dwarfs, ASP Conference Series, eds J.L. Provencal, H.L. Shipman, J. MacDonald, S. Goodchild. ASP San Francisco, p105.

Barstow M.A., Burleigh M.R., Banniser N.P., Holberg J.B., Hubeny I., Bruhweiler F.C., Napiwotzki R., 2001, 12th European Workshop on White Dwarfs, ASP Conference Series, eds J.L. Provencal, H.L. Shipman, J. MacDonald, S. Goodchild. ASP San Francisco, p128.

Barstow M.A., Hubeny I., Holberg J.B., 1998, MNRAS, 299, 520.

Barstow M.A., Hubeny I., Holberg J.B., 1999, MNRAS, 307, 884.

Barstow M.A., *et al.*, 1994a, MNRAS, 267, 647

Barstow M.A. *et al.*, 1994b, MNRAS, 271, 175

Barstow M.A., Holberg J.B., Cruise A.M., Penny A.J., 1997, MNRAS, 290, 505

Bergeron P., Saffer R. A., Liebert, J. 1992, ApJ, 394, 228

Bohlin R.C., Colina L., Finley D.S., 1995, AJ, 110, 1316

Bohlin R.C., 2000, AJ, 120, 437

Bruhweiler F.C, Barstow M.A., Holberg J.B., Sahu M., 2000, Bulletin of the American Astronomical Society, 195, 36.02

Burleigh M.R., Barstow M.A., Fleming T.A., 1997, MNRAS, 287, 318

Burleigh M.R., Barstow M.A., Schenker K.J., Sills A.I., Wynn G.A., Dobbie P.D., Good S.A., 2001, MNRAS, submitted

Dupuis J., Chayer P., Vennes S., Christian D.J., Kruk J.W., 2000, ApJ, 537, 977.

Dupuis J., Vennes S., Chayer P., Hurwitz M., Bowyer S., 1998, ApJ, 500, 45

Finley D.S., Koester D., Basri G., 1997a, ApJ, 488, 375

Finley D.S., Koester D., Kruk J.W., Kimble R.A., Allard N.F., 1997b, in White Dwarfs, ed.s J. Isern, M. Hernanz & E. Garcia-Berro (Kluwer, Dordrecht), p. 245

Green J.C., Wilkinson E., Friedman S.D., 1994, Proc SPIE, 2283, 12

Holberg J.B., Wesemael F., Basile J., 1986, ApJ, 306, 629

Holberg J.B., Wesemael F., Wegner G., Bruhweiler F.C., 1985, ApJ, 293, 294

Hubeny I., Lanz T., 1995, ApJ, 438, 875

Hubeny I., Lanz T., Jeffery C.S., 1994, CCP7 Newsletter on Analysis of Astronomical Spectra, Number 20, 30

Hurwitz M., Bowyer S., 1991, in Extreme Ultraviolet Astronomy, eds. R.F. Malina and S. Bowyer, Pergamon, New York, 442
Hurwitz M., Bowyer S., 1995, ApJ, 446, 812
Hurwitz, M., *et al.* 1998, ApJL, 500, L1
Koester D., Schulz H., Weidemann V., 1979, A& A, 76, 262
Kruk J.W., Brown T.M., Davidsen A.F., Espey B.R., Finley D.S., Kriss G.A., ApJS, 122, 299
Kruk J.W., Kimble R.A., Buss R.H., Davidsen A.F., Durrance S.T., Finley D.S., Holberg J.B., Kriss G.A., 1997, ApJ, 482, 546
Lanz T., Barstow M.A., Hubeny I., Holberg J.B., 1996, ApJ, 473, 1089.
Lemke M., 1997, A& A Suppl., 122, 285
Marsh, M.C. *et al.*, 1997, MNRAS, 286, 369
Moos, H.W., *et al.* 2000, ApJL, 538, L1
Shafer R.A., Haberl F., Arnaud K.A., Tennant A.F., 1991, ESA TM-09
Vennes S., Christian D.J., Thorstensen J.R., 1998, ApJ, 502, 763
Vennes S., Thejll P.A., Génova Galvan R., Dupuis J., 1997, ApJ, 480, 714
Vidal C.R., Cooper J., Smith E.W., 1973, ApJS, 25,37
Wood M.A., 1992, ApJ, 386, 539